Available online at www.sciencedirect.com
SCIENCE DIRECT®
Journal of Sound and Vibration 269 (2004) 61–89
JOURNAL OF SOUND AND VIBRATION
www.elsevier.com/locate/jsvi

Effect of high-frequency excitation on a class of mechanical systems with dynamic friction

S. Chatterjee*, T.K. Singha, S.K. Karmakar

Department of Mechanical Engineering, Bengal Engineering College, Deemed University, P.O. Botanic Garden, Howrah-711103, West Bengal, India

Received 9 August 2002; accepted 19 December 2002

Abstract

The effect of high-frequency excitation on a class of systems with friction is considered. Friction is represented by the LuGre and the elasto-plastic model of friction. Analytical expressions are obtained for the effective friction characteristics under two types of fast excitation. Numerical simulation using MATLAB validates the analytical results. The stability of a velocity tracking system with friction is discussed in light of the effective friction characteristics. Numerical simulation of a MATLAB™ SIMULINK model is carried out to unfold the basic physical mechanism underneath the mathematical expressions.

1. Introduction

Friction between two sliding surfaces plays a central controlling role in the dynamic behaviour of a number of systems. Various complex dynamical features like stick–slip motion, self–excited and chaotic oscillations are often identified with the presence of friction in joints and contact interfaces. Research on dynamical systems with friction has a long and rich history [1]. Recent advances in the precision mechatronic systems have brought a fresh impetus in the research interest on this topic. Except in a few cases, the side effects of friction lead to loss of functional accuracy of many systems and call for compensatory control arrangements. Though Coulomb's dry friction model is useful for the majority of rough engineering calculations, it is hardly suitable for some sophisticated applications because this model disregards the microscopic degrees of freedom of contact, which are important for some applications. For example, in precise mechatronic systems, the velocity and length scale of the motion becomes comparable to the

*Corresponding author.
E-mail address: shy@mech.becs.ac.in (S. Chatterjee).

0022-460X/03/$ - see front matter © 2003 Elsevier Ltd. All rights reserved.
doi:10.1016/S0022-460X(03)00004-X

length and time scale involved in the microscopic degrees of freedom of contact. Such understanding has led to the development of new phenomenological models of friction [2–4] and various compensation techniques. One of these compensation techniques considers high-frequency oscillation (dither) [5–7] in mitigating some evil effects of friction and shows a great deal of promise.

Engineers in reducing the effect of friction have used high-frequency oscillation long back [8,9]. However, only very recently, a systematic study of this effect has been initiated in a more general setup. Research [10–12] has revealed that any excitation operating at a time scale much faster compared to the natural time scale of a system may bring forth non-trivial changes in the dynamics of non-linear systems. In recent literature, such excitations are termed as fast vibration. Fast vibration have been shown to effectively change certain characteristics of mechanical systems such as equilibrium states [13], linear stiffness [14], damping [15] and natural frequencies [16]. Suitably designed fast excitation may also significantly influence certain non-linear features like restoring and energy dissipation characteristics, frequency response and bifurcation behaviour of non-linear systems. Another very important application of fast vibration is pivoted around the smoothening effect of the same on discontinuous system characteristics. Dry-friction characteristics are phemenologically described by a discontinuous fiction–velocity relationship, the discontinuity being at zero velocity, i.e., when velocity reversal takes place. Velocity reversal often involves sticking of two interacting surfaces, and during sticking phase, friction force assumes a value that depends on the external load. Thus, there exists a difference in the level of friction force in sticking and sliding phase. This is responsible for stick–slip motion. During low-velocity sliding, friction is shown to have drooping characteristics with increasing velocity. This is known as Stribeck effect, and responsible for self-excited oscillation of various systems. Thomsen [5] considers a similar model of friction to investigate into the effect of fast excitation on stick–slip dynamics. It is shown that a properly chosen fast vibration is capable of suppressing self-excited oscillation and stick–slip motion. Due to the effect of fast-vibration the zero-velocity discontinuity of friction force is removed by an equivalent viscous damping characteristics, and the low-velocity drooping characteristic tends to flatten out simultaneously. Feeny and Moon [6] have experimentally demonstrated the possibility of using fast vibration in quenching friction-driven chaos. Tuned dither has also been successfully applied in eliminating friction-induced error in robotic manipulators [7].

A great number of recent phenomenological friction models consider only the macroscopic degrees of freedom. This implies that all microscopic degrees of freedom are much faster than the macroscopic ones. Such an assumption breaks loose when the velocity of sliding becomes comparable to the ratio of microscopic length scale to macroscopic time scale [17]. This microscopic length scale may be of the same order of magnitude as the size of the asperities of the contact surface or the correlation length of the surface roughness. Therefore, when velocity becomes very low, one has to pay attention also in the microscopic degrees of freedom, which are in general faster in dynamics. Moreover, coming to the understanding of the effect of fast vibration, consideration of the interaction of fast microscopic degrees of freedom and the fast excitation becomes important. Few recent models of friction incorporate the microscopic degrees of freedom, and such models are known as dynamic models of friction [2–4]. In the present paper, the effect of fast vibration on the dynamics of a class of systems represented by dynamic models of friction is investigated. For the present investigation, the LuGre [2] and the single-state

elasto-plastic models of friction [3] are considered. The effect of fast vibration on the stick–slip, and self-excited oscillation has been discussed in the light of fast vibration-induced effective friction characteristics. Detail numerical simulation is carried out to understand the mechanism of the effect of fast vibration on friction-driven dynamics. The organisation of the paper is briefly given below.

The discussion starts with a brief review of the existing mathematical models of friction in Section 2. Section 3 deals with a simple non-inertial contact model considering only the microscopic degrees of freedom of the contact, and the effect of high-frequency velocity variation is studied by the method of harmonic balance. In Section 4, an example system consisting of an elastic slider moving on a frictional surface is considered. The slider is modelled as a single-degree-of-freedom system and the frictional contact is modelled according to the LuGre dynamic friction model. In Section 5, the effect of high-frequency excitation on the friction characteristics of the example system discussed in Section 4 is studied analytically. Two different kinds of fast excitation, namely sinusoidal force excitation and square wave velocity excitation are considered for analytical estimation of the effective friction characteristics. Analytical results are also compared with that obtained from the direct numerical simulation of the system. The effect of fast-excitation on stick–slip instability of the system is considered in Section 6. In Section 7, a more rigorous elasto-plastic model of friction is considered for numerical investigation into the mechanism of the effect of fast excitation on stick–slip motion.

2. Models of friction

Modern literature is rich in significantly large number of mathematical models of friction. Each of these models is relevant only for one or few phenomenology and operating ranges of its own interest. For a particular problem, selection of the appropriate friction model is very important. Depending on the length and time scale involved, the existing models of friction in literature can be classified into two broad categories, namely macroscopic and microscopic models.

In macroscopic models, friction is represented as a dissipative function of relative velocity of sliding. Such models are mainly valid in situations where only macroscopic structural degrees of freedom involving relatively slower time scale are of paramount importance. The simplest form of such macroscopic models is the Coulomb's dry friction model given as follows:

$$F = F_c \,\mathrm{Sgn}(v). \tag{2.1}$$

This model only recognises the fact that friction force F is constant and depends on the sign of relative sliding velocity. However, Coulomb's model cannot describe the stick–slip or the Stribeck effect. There exist a number of extensions of Coulomb's model, which consider the stick–slip and the Stribeck effect. Such models are called kinetic friction models (KFM) and may in general be given by

$$F = \begin{Bmatrix} g(v), & v \neq 0 \\ F_e & \text{if } v = 0 \text{ and } |F_e| < F_s \\ F_s \,\mathrm{Sgn}(F_e) & \text{otherwise} \end{Bmatrix}, \tag{2.2}$$

where

$$g(v) = F_c + (F_s - F_c)e^{|v/v_s|^\delta} + F_v v.$$

In Eq. (2.2), F_e is the external force, F_s is the maximum level of multi-valued friction force during sticking and F_c is the kinetic friction force. vs is the characteristic Stribeck velocity and F_v is the viscous friction coefficient.

In recent times, a series of sophisticated models friction have been developed considering the microscopic degrees of freedoms of friction interface. Such models are known as 'bristle models', where asperities of the friction interface are considered as elastic spring-like bristles. When a tangential force is applied, the bristles deflect like springs, and the friction force is represented as the average deflection force of the spring-like bristles. When deflection of the bristles is sufficiently large, the bristles start slipping. The velocity of sliding determines the average deflection during steady slipping. The LuGre model [2] is the most widely used form of microscopic model of friction that relies on bristles interpretation. Recently, Dupont et al. [3] further generalise the LuGre model to incorporate stiction phenomena in a more rigorous manner. The generalised LuGre model, known as the 'single-state elasto-plastic model' is described as

$$\begin{aligned} F &= \sigma_0 z + \sigma_1 \frac{dz}{dt} + \sigma_2 v, \quad \sigma_0, \sigma_1, \sigma_2 > 0, \\ \frac{dz}{dt} &= v - \frac{\sigma_0 \alpha(z, v)|v|z}{g(v)}, \end{aligned} \tag{2.3}$$

where v is the relative velocity between the matting surfaces and z is the average deflection of the bristles. $g(v)$ models the Stribeck effect and the most common form of $g(v)$ is as follows:

$$g(v) = F_c + (F_s - F_c)e^{-|v/v_s|^\delta}. \tag{2.4}$$

σ_0 and σ_1 represents bristle stiffness and damping, respectively. σ_2 is viscous damping coefficient and v_s is the characteristic Stribeck velocity. To render the model dissipative, the bristle damping term σ_1 is taken to be a function of velocity. The most common form of this function is given by

$$\sigma_1(v) = \hat{\sigma}_1 e^{-|v/v_d|^\delta}, \tag{2.5}$$

where v_d is a characteristic velocity and d is a positive quantity, and these two parameters models the rate of change of bristle damping with sliding velocity. The function $\alpha(z, v)$ (introduced by Dupont et al. [3]) controls different phases of friction process like sticking, elasto-plastic pre-sliding and pure sliding by assuming different values at different states as follows:

$$\begin{aligned} \alpha(z, v) &= \left\{ \begin{array}{ll} 0 & \text{for } |z| < z_{ba} \\ \alpha_m(z, z_{ba}, z_{ss}) & \text{for } z_{ba} < |z| < z_{ss}(v) \\ 1 & \text{for } |z| > z_{ss}(v) \end{array} \right\} \quad \text{when } \mathrm{Sgn}(v) = \mathrm{Sgn}(z) \\ &= \{0\} \qquad\qquad\qquad\qquad\qquad\qquad\quad \text{when } \mathrm{Sgn}(v) \neq \mathrm{Sgn}(z), \end{aligned} \tag{2.6}$$

$$\text{where } 0 < \alpha_m(.) < 1 \text{ and } z_{ss}(v) = \frac{g(v)}{\sigma_0}.$$

Dupont et al. [3] suggest the following form of the function $\alpha_m(.)$.

$$\alpha_m(z, z_{ba}, z_{ss}(v)) = \frac{1}{2}\sin\left(\pi\frac{z - \frac{z_{ss}+z_{ba}}{2}}{z_{ss} - z_{ba}}\right) + \frac{1}{2} \tag{2.7}$$

The above form of the function $\alpha(z, v)$ clearly suggests that during sticking when bristle deflection z is less than z_{ba} (the breakaway deflection) $\alpha(z, v) = 0$. After that elasto-plastic pre-sliding begins when $\alpha(z, v) = \alpha_m(.)$ and this phase continues unto $z = z_{ss}(v)$ (maximum steady-state bristle deflection at velocity v). Then full plastic slipping follows when $\alpha(z, v) = 1$.

It is to be noted that the LuGre model may be simulated by putting $\alpha(z, v) = 1$ in Eq. (2.3). Thus, the LuGre model cannot rigorously capture complete stiction during which the bristle deflection is expected to be purely elastic (as in case of the elasto-plastic model). Numerical simulation of systems with the LuGre friction model shows slow drift of the slider during stiction phase. This is similar to the elasto-plastic pre-sliding observed in case of the elasto-plastic model.

3. Effect of harmonically varying unidirectional velocity on friction characteristics: contact model without inertia

As friction is strongly dependent on velocity, any effect of high-frequency excitation on friction takes place through high-frequency velocity variation. In order to understand the effect of high-frequency velocity variation on friction, a hypothetical contact model is considered where a slider is moving with a constant velocity (v_m), and a velocity perturbation of the form $v_a\cos(\omega t)$ (with $v_a <= v_m$) is superimposed on it. For a simplified analysis, the macroscopic degrees of freedom of the slider are neglected in the model. The LuGre friction model represents the friction characteristic. As discussed earlier, the LuGre friction model is a special case of elasto-plastic model described in Eqs. (2.3)–(2.7) and simulated by putting $\alpha(.) = 1$. For mathematical convenience, the Stribeck effect is modelled by putting $\delta = 1$ in Eq. (2.4). The harmonic balance method (HBM) is used to analyze the friction characteristic under high-frequency velocity variation. In this method, the bristle deflection z is represented by Fourier series expansion as given below (see Appendix A for details).

$$z = X_0 + \sum_{n=1}^{H} X_n\cos(n\omega t) - \sum_{n=1}^{H} Y_n\sin(n\omega t), \tag{3.1}$$

where H is the number of harmonic terms used in the expansion. X_0, X_n and Y_n are calculated from the following linear equation:

$$[A]\{\vec{\xi}\} = \{\vec{b}\}, \tag{3.2}$$

where

$$\{\vec{\xi}\} = \{X_0\, X_1 \ldots X_H \quad Y_1\, Y_2 \ldots Y_H\}^{\mathrm{T}}$$

$$\{\vec{b}\} = \{Q_0 Q_1 \ldots Q_H \;\; 0\; 0 \ldots 0\}^{\mathrm{T}}.$$

In Eq. (3.2), the elements of the $(2H + 1) \times (2H + 1)$ matrix $[A]$ and the vector $\{b\}$ are functions of the model parameters α_0, α_1, σ_0, σ_1, σ_2, v_m, v_a, ω, v_0 and v_d. Finally, the friction force is

computed by

$$F = \sigma_0 z + \sigma_1(v)\frac{\mathrm{d}z}{\mathrm{d}t} + \sigma_2 v. \tag{3.3}$$

Out of various phenomena captured by the LuGre friction model, only the memory effect and the Stribeck effect are relevant for the present discussion. The memory effect of friction is identified with the existence of a closed loop in the friction-velocity plot. Eqs. (3.1)–(3.3) are solved and the friction vs. velocity characteristics are shown in Fig. 1 for various frequency of velocity variation. While solving Eqs. (3.1)–(3.3), the mean velocity v_m and the amplitude of velocity perturbation v_a are set to be equal. Under such circumstances, the sliding velocity instantaneously comes down to zero at a certain instant of velocity history. However, as macroscopic degrees of freedom of the slider is not considered in the model, instantaneous zero velocity should not be confused with the stiction phenomenon (stiction is addressed elsewhere in the paper). From Fig. 1, it is observed that the frequency of velocity variation has a significant effect on the shape and size of the memory loop. The size of the loop initially increases with the frequency and then gradually shrinks down. At a very high frequency, an asymptotic friction characteristic with negligibly small loop area is obtained. The friction force near zero velocity uniformly decreases with the increasing frequency of velocity variation. A pertinent relationship between the bristle stiffness σ_0 (i.e. on the tangential contact compliance) and the frequencies at which the friction force approaches the asymptotic characteristics is also observed (results are not presented). In case of higher stiffness of bristles, higher frequency is required to obtain the asymptotic friction characteristic.

The frequency compositions of the friction force under harmonically varying unidirectional velocity are shown in Fig. 2. From this figure, it is observed that high frequency of velocity variation causes strong attenuation of the higher harmonic contents of the friction force. This result gives a frequency domain picture of the smoothening effect of high-frequency excitation on non-smooth friction process.

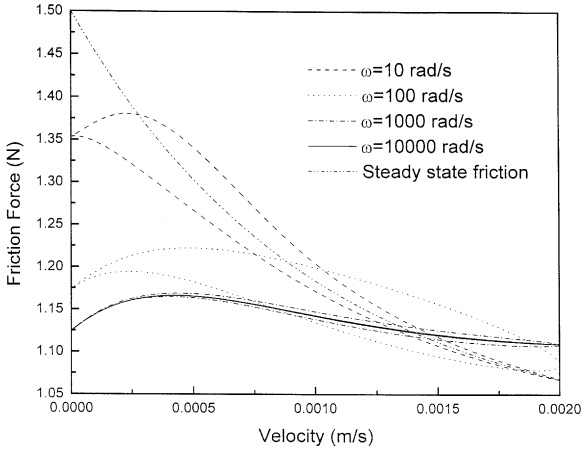

Fig. 1. Effect of the frequency of velocity variation on friction characteristics. $\sigma_0 = 1 \times 10^5$ N/m, $\sigma_1 = 1 \times 10^3$ N/m/s, $\sigma_2 = 0$, $F_s = 1.5$ N, $F_c = 1$ N, $v_s = v_d = 0.001$ m/s, $v_m = v_a = 0.001$ m/s.

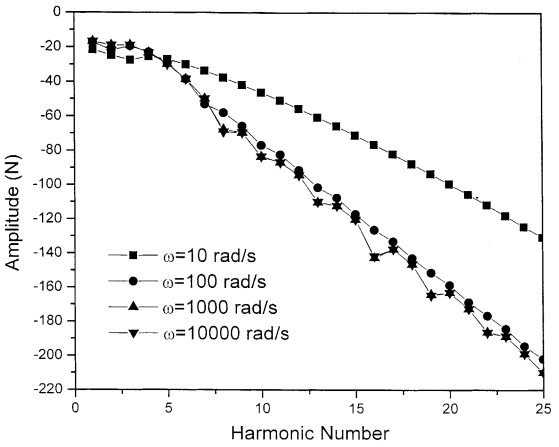

Fig. 2. Change of frequency composition of friction force with the frequency of velocity variation. $\sigma_0 = 1 \times 10^5$ N/m, $\sigma_1 = 1 \times 10^3$ N/m/s, $\sigma_2 = 0$, $F_s = 1.5$ N, $F_c = 1$ N, $v_s = v_d = 0.001$ m/s, $v_m = v_a = 0.001$ m/s.

It is important to note here that the source of instability in dynamic systems with friction is often related to the drooping characteristics of friction with increasing velocity. The results of the present analysis suggest that high-frequency velocity fluctuation can change the slope of very low-velocity friction characteristics from negative to positive. Thus, friction-induced instability in dynamic systems may be controlled by high frequency velocity perturbation. This also explains the fact that friction-induced instability is absent in stiff systems because in stiff systems oscillation of velocity takes place at high frequency. Results of this section confirm and extend the already known results [5] (for some macroscopic friction models) also for the microscopic friction models. However, it is to be kept in mind that the contact model considered in this section is highly idealised as the macroscopic degrees of freedom (the inertia of the slider mass) is not taken into account. Therefore, the effect of high-frequency velocity perturbation at many important phases of motion like stiction and stick–slip phase is not explained in the capacity of the present model. In what follows, realistic contact models with coupled macro and microscopic degrees of freedom are considered.

4. Mathematical model of an example system with dynamic friction

Mathematical model of a single-degree-of-freedom system with friction is shown in Fig. 3, where an elastic slider (moving on a frictional surface) having a mass m coupled by stiffness k to a drive capable of producing time-varying velocity command of the form $v_m + v_a(t)$. The system is subjected to friction represented mathematically according to the LuGre dynamic friction model. The slider is excited by a high-frequency excitation. The frequency of excitation is very large compared to the natural frequency of the system or the frequency of variation of the velocity command. Non-dimensional equation of motion of the system

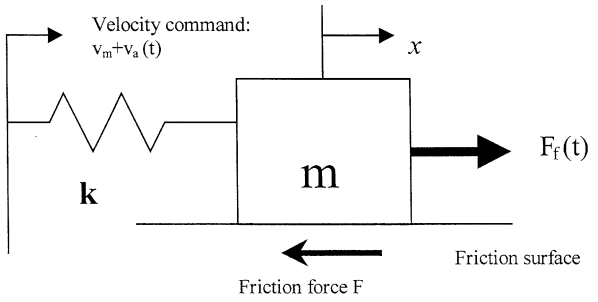

Fig. 3. Mathematical model of the system under consideration.

is given by

$$\ddot{X} + X + \tilde{F} = \tilde{f}_f(\tau, T_0) + \tilde{f}_s(\tau) + v_m^* \tau,$$

$$\frac{\mathrm{d}Z}{\mathrm{d}\tau} = \dot{X} - \frac{\sigma_0^* |\dot{X}| Z}{g^*(\dot{X})}$$

and

$$\tilde{F} = \sigma_0^* Z + \sigma_1^*(\dot{X}) \frac{\mathrm{d}Z}{\mathrm{d}\tau} + \sigma_2^* \dot{X}, \tag{4.1}$$

where the non-dimensional quantities are as defined below.
$\tau = t\omega_n$ is non-dimensional time, $T_0 (\ll 1)$ is non-dimensional time period of fast excitation.

$$\tilde{f}_f(\tau, T_0) = \frac{F_f}{m\omega_n^2 L}$$

and

$$\tilde{f}_s(\tau) = \frac{k \int_0^\tau v_a(s)\,\mathrm{d}s}{m\omega_n^2 L}$$

are fast (dither) and slow excitation, respectively.

$$\omega_n = \sqrt{\frac{k}{m}},$$

$X = x/L, \dot{X} = x/\omega_n L, \ddot{X} = x/\omega_n^2 L$, $Z = z/L$ with L as an arbitrary length quantity;

$$\sigma_0^* = \frac{\sigma_0}{k}, \sigma_1^*(\dot{X}) = \hat{\sigma}_1^* \mathrm{e}^{-(\dot{X}/v_d^*)^2}, \quad \hat{\sigma}_1^* = \frac{\hat{\sigma}_1}{m\omega_n}, v_d^* = \frac{v_d}{\omega_n L}, \quad \sigma_2^* = \frac{\sigma_2}{m\omega_n}$$

and

$$g*(\dot{X}) = f_c + (f_s - f_c)\mathrm{e}^{-(\dot{X}/v_s^*)^2}$$

with

$$f_c = \frac{F_c}{m\omega_n^2 L}, f_s = \frac{F_s}{m\omega_n^2 L}, v_m^* = \frac{v_m}{\omega_n L} \quad \text{and} \quad v_s^* = \frac{v_s}{\omega_n L}.$$

In the above model, X represents the macroscopic structural degree of freedom and Z (deflection of interface bristles) represents the microscopic degree of freedom of the friction

interface. These two degrees of freedom are coupled through the friction force. The equation of motion (4.1) without the fast excitation generally describes the dynamics in two disparate time scales, Z being the faster variable. Three disparate time–scales may appear when the time scale of the fast excitation is different from the time scales of X and Z.

5. Theoretical estimation of the effective friction under fast vibration

In this section, two different models of fast excitation are considered to analyze the effective friction characteristics. The first model deals with a somewhat hypothetical but theoretically possible fast excitation, which is equivalent to driving the frictional surface by high-frequency velocity excitation. The consideration of this type of excitation makes the system amenable to easy analytical treatment. The second model uses sinusoidal fast excitation, and considers a relatively simpler version of friction model in obtaining an analytical expression of the effective friction characteristics. Though sinusoidal excitation is more realistic, the corresponding analytical treatment becomes tedious when a complete model of friction is considered. Therefore, for the mathematical convenience, only a partial model (keeping only the essential part) of friction is considered in this case. However, it will be shown later that qualitatively as well as quantitatively one does not miss much even with this partial model of friction.

5.1. Model 1: fast excitation is equivalent to square wave velocity excitation

As the effective friction characteristics are of importance, one sets v_m* equal to zero. Under this circumstance, the non-dimensional equation of motion of the system may be written as

$$\ddot{X} + X + \tilde{F} = \tilde{f}_f(\tau, T_0) + \tilde{f}_s(\tau),$$
$$\frac{\mathrm{d}Z}{\mathrm{d}\tau} = \dot{X} - \frac{\sigma_0^*|\dot{X}|Z}{g^*(\dot{X})},$$

and

$$\tilde{F} = \sigma_0^* Z + \sigma_1^*(\dot{X})\frac{\mathrm{d}Z}{\mathrm{d}\tau} + \sigma_2^*\dot{X}. \tag{5.1}$$

If the fast excitation is assumed much faster compared to both X and Z, it is pertinent to represent the system into two disparate time scales. Therefore, one can use the method of direct partition of motion (MDPM) [18] to split the motion X and Z into slow and fast components, the time scale of the fast component having the same order of magnitude as the fast excitation. Thus, one writes

$$X(\tau) = X_s(\tau) + T_0\phi_1(\tau, T),$$
$$Z(\tau) = Z_s(\tau) + T_0\phi_2(\tau, T), \tag{5.2}$$

where

$$T = T_0^{-1}\tau,$$

with

$$\langle \phi_{1,2} \rangle = T_0^{-1} \int_0^{T_0} \phi_{1,2}(\tau, T)\, \mathrm{d}T = 0. \tag{5.3}$$

Putting Eq. (5.2) in Eq. (5.1), one obtains

$$\phi_1'' = -T_0(\ddot{X}_s + 2\dot{\phi}_1' + X_s + \tilde{F} - \tilde{f}_s(\tau)) + T_0 \tilde{f}_f(\tau, T_0) + O(T_0^2) \tag{5.4a}$$

$$\phi_2' = -\dot{Z}_s + \dot{X}_s + \phi_1' - \frac{\sigma_0^* |\dot{X}_s + \phi_1'| Z_s}{g^*(\dot{X}_s + \phi_1')} + O(T_0), \tag{5.4b}$$

where $'$ denotes differentiation with respect to time variable T.

If the fast excitation is strong enough such that

$$T_0 \tilde{f}_f(\tau, T_0) \sim \mathrm{O}(1) \text{ or higher},$$

the first order form of Eq. (5.4a) is given by

$$\phi_1'' = T_0 \tilde{f}_f(\tau, T_0). \tag{5.5}$$

For mathematical convenience, one may assume that there exists a fast excitation force (at least theoretically) such that single integration of Eq. (5.5) gives a square pulse. Thus, ϕ_1' is represented by a square pulse as shown in Fig. 4. One should note that the application of such fast excitation produces the same effect as obtained by superimposing a high-frequency square-wave on the sliding velocity. Using Eq. (5.3), one can perform averaging of Eqs. (5.4a) and (5.4b) to obtain the following equations that govern the average dynamics of the system:

$$\ddot{X}_s + X_s + \langle \tilde{F}(Z_s, \dot{X}_s + \phi_1') \rangle = \tilde{f}_s(\tau), \tag{5.6a}$$

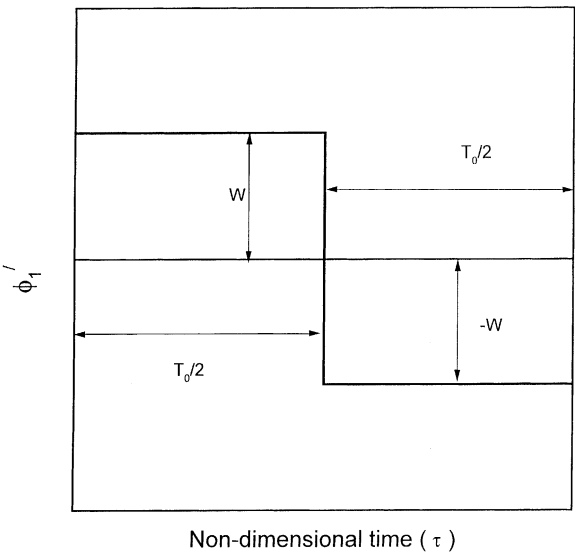

Fig. 4. High-frequency square wave.

$$\dot{Z}_s = \dot{X}_s - \sigma_0^* Z_s \left\langle \frac{|\dot{X}_s + \phi_1'|}{g^*(\dot{X}_s + \phi_1')} \right\rangle$$
$$= \dot{X}_s - \frac{1}{2}\sigma_0^* Z_s \left(\frac{|\dot{X}_s + W_1|}{g^*(\dot{X}_s + W)} + \frac{|\dot{X}_s - W|}{g^*(\dot{X}_s - W)} \right), \tag{5.6b}$$

where

$$\langle \tilde{F} \rangle = \sigma_0^* \left(1 - \left\langle \frac{\sigma_1^*(\dot{X}_s + \phi_1')|\dot{X}_s + \phi_1'|}{g^*(\dot{X}_s + \phi_1')} \right\rangle \right) Z_s + \left(\sigma_2^* \dot{X}_s + \langle \sigma_1^*(\dot{X}_s + \phi_1')(\dot{X}_s + \phi_1') \rangle \right)$$
$$= \sigma_0^* Z_s + \sigma_2^* \dot{X}_s + \frac{1}{2}\left(\sigma_1^*(\dot{X}_s + W)(\dot{X}_s + W) + \sigma_1^*(\dot{X}_s - W)(\dot{X}_s - W) \right)$$
$$- \frac{1}{2}\sigma_0^* Z_s \left(\frac{\sigma_1^*(\dot{X}_s + W)|\dot{X}_s + W|}{g^*(\dot{X}_s + W)} + \frac{\sigma_1^*(\dot{X}_s - W)|\dot{X}_s - W|}{g^*(\dot{X}_s - W)} \right). \tag{5.6c}$$

It is pertinent to assume that non-dimensional contact stiffness $\sigma_0^* \gg 1$. Thus, Eqs. (5.6a)–(5.6c) may be rewritten as

$$\ddot{X}_s + X_s + \langle \tilde{F}(Y, \dot{X}_s + \phi_1') \rangle = \tilde{f}_s(\tau), \tag{5.7a}$$

$$\varepsilon \dot{Y} = \dot{X}_s - \frac{1}{2} Y \left(\frac{|\dot{X}_s + W_1|}{g^*(\dot{X}_s + W)} + \frac{|\dot{X}_s - W|}{g^*(\dot{X}_s - W)} \right), \tag{5.7b}$$

where

$$\langle \tilde{F} \rangle = Y + \sigma_2^* \dot{X}_s + \frac{1}{2}\left(\sigma_1^*(\dot{X}_s + W)(\dot{X}_s + W) + \sigma_1^*(\dot{X}_s - W)(\dot{X}_s - W) \right)$$
$$- \frac{1}{2} Y \left(\frac{\sigma_1^*(\dot{X}_s + W)|\dot{X}_s + W|}{g^*(\dot{X}_s + W)} + \frac{\sigma_1^*(\dot{X}_s - W)|\dot{X}_s - W|}{g^*(\dot{X}_s - W)} \right), \tag{5.7c}$$

where

$$Y = \sigma_0^* Z_s \text{ and the small quantity } \varepsilon = (\sigma_0^*)^{-1}.$$

One observes that Eqs. (5.7a) and (5.7b) are in the standard form of singular- perturbation problem. Thus, following Tikhonov theorem [19], the corresponding dynamics can be described on slow and fast manifolds. It may be noted here that the structural degree of freedom X_s describes the slow dynamics and the microscopic degree of freedom Y describes the fast dynamics of the system. Putting $\varepsilon = 0$ in Eq. (5.7b), one obtains the reduced order model of the system as follows:

$$\ddot{X}_s + X_s + \langle \tilde{F}(Y, \dot{X}_s + \phi_1') \rangle = \tilde{f}_s(\tau), \tag{5.8}$$

where the effective friction force $\langle \tilde{F} \rangle$ is given by

$$< \tilde{F} > = Y + \sigma_2^* \dot{X}_s + \frac{1}{2}(\sigma_1^*(\dot{X}_s + W)(\dot{X}_s + W) + \sigma_1^*(\dot{X}_s - W)(\dot{X}_s - W))$$
$$- \frac{1}{2} Y \left(\frac{\sigma_1^*(\dot{X}_s + W)|\dot{X}_s + W|}{g^*(\dot{X}_s + W)} + \frac{\sigma_1^*(\dot{X}_s - W)|\dot{X}_s - W|}{g^*(\dot{X}_s - W)} \right), \tag{5.9}$$

and

$$Y = \frac{2\dot{X}_s}{\left(\dfrac{|\dot{X}_s + W|}{g^*(\dot{X}_s + W)} + \dfrac{|\dot{X}_s - W|}{g^*(\dot{X}_s - W)}\right)}. \tag{5.10}$$

Eq. (5.10) describes the slow manifold of the system. After using the following time and co-ordinate transformation

$$\hat{Y} = Y - \frac{2\dot{X}_s}{\left(\dfrac{|\dot{X}_s + W_1|}{g^*(\dot{X}_s + W)} + \dfrac{|\dot{X}_s - W|}{g^*(\dot{X}_s - W)}\right)}, \hat{\tau} = \tau/\varepsilon$$

and considering $\dot{X}_s$ as constant one obtains the boundary layer system describing the fast dynamics as

$$\frac{\mathrm{d}\hat{Y}}{\mathrm{d}\hat{\tau}} = -\frac{1}{2}\hat{Y}\left(\frac{|\dot{X}_s + W_1|}{g^*(\dot{X}_s + W)} + \frac{|\dot{X}_s - W|}{g^*(\dot{X}_s - W)}\right). \tag{5.11}$$

One may observe that the equilibrium

$$\hat{Y} = 0$$

of boundary layer problem (5.11) is uniformly asymptotically stable for all velocities. Therefore, according to the Tikhonov's theorem[1], the reduced problem given by Eqs. (5.8)–(5.10) describes the steady state dynamics of X_s accurate to order ε.

As a numerical example, typical plots of the effective friction vs. velocity are shown in Fig. 5 for the following parameter values (suitably non-dimensionalised experimental data [2]).

$$\sigma_0^* = 100, \quad \hat{\sigma}_1^* = 10, \quad \sigma_2^* = 0.004, \quad v_s^* = 0.1, \quad f_c = 1, \quad f_s = 1.5.$$

As discussed earlier, v_d^* renders the friction model dissipative by controlling the rate of change of bristle damping factor with velocity. However, no experimental value of the parameter v_d^* is available in literature. Theoretically, one may assume any value that satisfies the following condition:

$$\sigma_1^*(v) < \frac{4g^*(v)}{|v|}.$$

In the present discussion, two different values of v_d^* are used. In Fig. 5(a), v_d^* is of the same order of magnitude as v_s^* and is one order less in Fig. 5(b). It is noted from Fig. 5(b) that for small values of v_d^*, one may neglect the effect bristle damping and obtain a simplified expression of the effective friction force as follows:

$$\langle \tilde{F} \rangle = \frac{2\dot{X}_s}{\left(\dfrac{|\dot{X}_s + W|}{g^*(\dot{X}_s + W)} + \dfrac{|\dot{X}_s - W|}{g^*(\dot{X}_s - W)}\right)} + \sigma_2^* \dot{X}_s \tag{5.12}$$

[1] The other Tikhonov conditions are also satisfied almost everywhere except when absolute value of the sliding velocity is W.

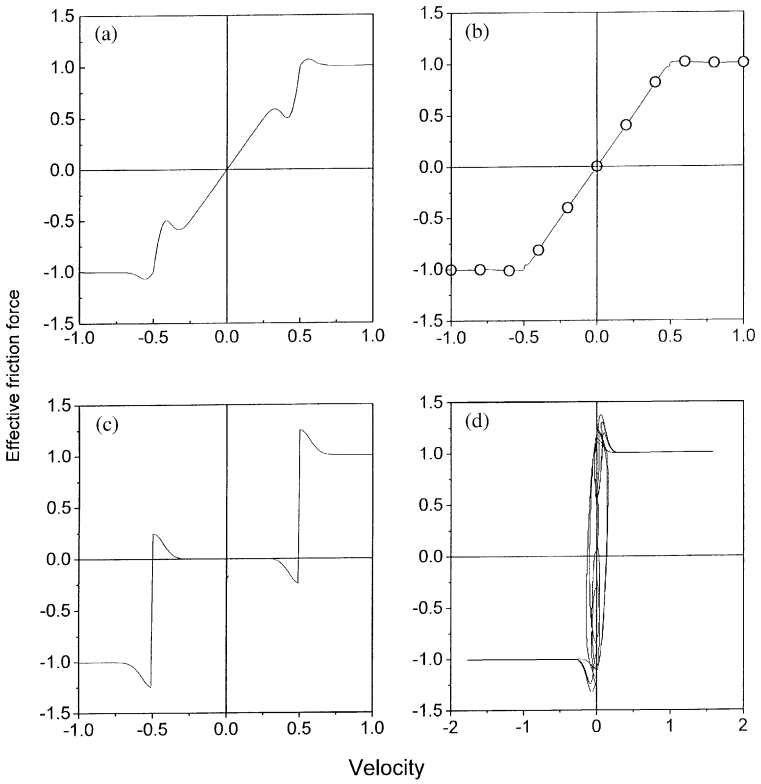

Fig. 5. Analytically obtained effective friction force with and without fast excitation discussed in model 1. (a) LuGre model, $v_d^* = 0.1$; (b) LuGre model, $v_d^* = 0.01$; (c) static friction model and (d) without dither (LuGre).

Corresponding effective friction force obtained from Eq. (5.12) is shown in Fig. 5(b) (as o-markers). From Figs. 5(a) and (b), it is observed that in the low-velocity ($\ll W$) region effective friction force acts like almost linear viscous damping force. In the high-velocity region, friction characteristics follow the viscous damping characteristics of the lubricated surface. Therefore, one may write

$$\frac{\mathrm{d}\langle \tilde{F} \rangle}{\mathrm{d}\dot{X}_s} = \frac{f_c + W\sigma_2^*}{W} \quad \forall\, |\dot{X}_s| \ll W,$$

$$\frac{\mathrm{d}\langle \tilde{F} \rangle}{\mathrm{d}\dot{X}_s} \approx \sigma_2^* \quad \forall |\dot{X}_s| \gg W. \tag{5.13}$$

From Eq. (5.13), one infers that the effective low-velocity friction characteristic is a function of the Coulomb level of friction force, viscous damping coefficient of the lubricated surface and the dither characteristics.

In case of higher value of v_d^*, one observes (Fig. 5(a)) a transitional complexity in the effective friction vs. velocity characteristics around the dither velocity W. Besides the primary negative slope in friction vs. velocity plot associated with the Stribeck effect, one observes a secondary zone of negative slope. This secondary zone occurs at velocity less than W, whereas the primary zone of

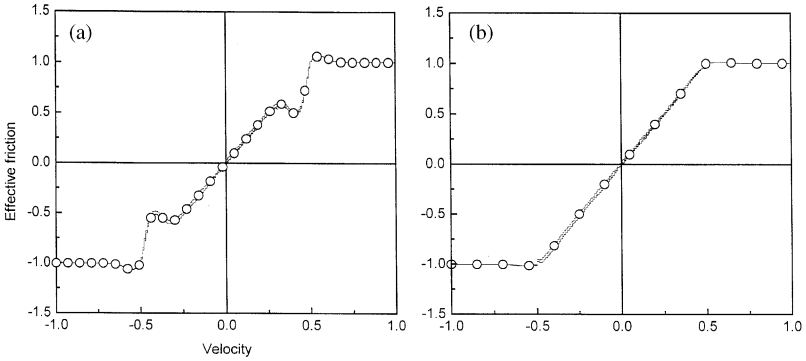

Fig. 6. Comparison of analytical and simulated effective friction characteristics. ——, MATLAB simulation; ○, analytical. (a) $v_d^* = 0.1$, (b) $v_d^* = 0.01$.

negative slope occurs at velocity higher than W. The effect of this secondary zone of negative slope on the stability of the system is addressed elsewhere in the article.

It is important to note the difference between the effective friction characteristics calculated based on the steady state friction model and the LuGre model. In case of the steady state friction model, the effective friction characteristic is given by

$$\langle \tilde{F} \rangle = 0.5(g^*(\dot{X}_s + W)\mathrm{Sgn}(\dot{X}_s + W) + g^*(\dot{X}_s - W)\mathrm{Sgn}(\dot{X}_s - W)) + \sigma_2^* \dot{X}_s. \tag{5.14}$$

Corresponding effective friction vs. velocity is plotted in Fig. 5(c) for comparison. From Fig. 5(c), it is observed that the slope of the effective friction force calculated form the steady state model is σ_2^* and thus, independent of the dither characteristics (W). When no lubrication is used, i.e., $\sigma_2^* = 0$, the low velocity friction force becomes zero. Therefore, one infers that the steady state friction model underestimates the effective friction force in comparison to that obtained from the LuGre model.

To verify the analytical results discussed above, numerical simulation of the system is carried out using MATLAB™ SIMULINK. The slow excitation is modelled as $1.7\sin(0.5\tau)$ and the dither (superimposed on the velocity of the slider) as a square waveform having amplitude 0.5 and frequency 1000. The effective friction forces vs. velocity characteristics are constructed using the filtered versions of velocity and friction. Low-pass Butterworth analog filters (filter order 8 and the lower band edge frequency 500) are used to eliminate the high-frequency components of velocity and friction signal. Numerically simulated (using the Dormand-Prince algorithm) effective friction characteristics depicted in Figs. 6(a) and (b) clearly demonstrates the validity of the analytical results shown in Figs. 5(a) and (b).

5.2. *Model 2: sinusoidal dither*

A comprehensive theoretical analysis presented in the last section has demonstrated that the low-velocity effective friction characteristics is a strong function of the Coulomb friction level, viscous damping characteristics of the lubricated surface and the dither characteristics. In the present section, a simplified model of friction, disregarding the Stribeck effect and the bristle damping, is considered to analyze the effect of sinusoidal dither on the low-velocity friction

characteristics. Under these circumstances, equation of motion (5.1) assumes the following form:

$$\begin{aligned} \ddot{X} + X + \tilde{F} &= \tilde{f}_s(\tau) + a\Omega_f^2 \sin(\Omega_f \tau), \\ \dot{Z} &= \dot{X} - \frac{\sigma_0^* |\dot{X}| Z}{f_c}, \end{aligned} \tag{5.15}$$

where the friction force $\tilde{F}$ is given by

$$\tilde{F} = \sigma_0^* Z + \sigma_2^* \dot{X}.$$

According to the theory of MDPM, on writes

$$\begin{aligned} X(\tau) &= X_s(\tau) + \Omega_f^{-1} \phi_1(\tau, T), \\ Z(\tau) &= Z_s(\tau) + \Omega_f^{-1} \phi_2(\tau, T), \end{aligned} \tag{5.16}$$

where

$$T = \Omega_f \tau,$$

with

$$\langle \phi_{1,2} \rangle = \frac{1}{2\pi} \int_0^{2\pi} \phi_{1,2}(\tau, T)\, \mathrm{d}T = 0. \tag{5.17}$$

Using the similar assumptions and methods discussed in Section 5.1, one obtains the average dynamics of the system as follows:

$$\begin{aligned} \ddot{X}_s + X_s + \sigma_0^* Z_s + \sigma_2^* \dot{X}_s &= \tilde{f}_s(\tau), \\ \dot{Z}_s &= \dot{X}_s - \frac{\sigma_0^* Z_s \langle |\dot{X}_s + \phi_1'| \rangle}{f_c}, \end{aligned} \tag{5.18}$$

where

$$\phi_1' = -a\Omega_f \cos(\Omega_f \tau).$$

After computation of the average $\langle \cdot \rangle$, Eq. (5.18) takes the following form:

$$\ddot{X}_s + X_s + \sigma_0^* Z_s + \sigma_2^* \dot{X}_s = \tilde{f}_s(\tau),$$

$$\dot{Z}_s = \dot{X}_s - \frac{\sigma_0^* Z_s}{f_c} \{ 2a\Omega_f \sin(\theta_1) + \dot{X}_s(\pi - 2\theta_1) \}, \quad \text{with} \quad \theta_1 = \cos^{-1}\left(\frac{\dot{X}_s}{a\Omega_f} \right) \text{ when } |\dot{X}_s| \leqslant a\Omega_f, \tag{5.19a}$$

and

$$\dot{Z}_s = \dot{X}_s - \frac{\sigma_0^* Z_s}{f_c} |\dot{X}_s|, \quad \text{when } |\dot{X}_s| > a\Omega_f. \tag{5.19b}$$

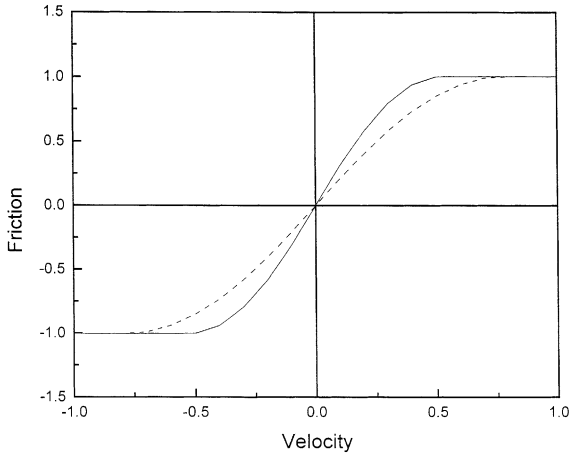

Fig. 7. Effective friction characteristics with sinusoidal dither. ——, $a\Omega_f = 0.5$; ------, $a\Omega_f = 0.75$.

One finally obtains the effective friction characteristics as

$$\begin{aligned}\langle \tilde{F} \rangle &= \sigma_0^* Z_s + \sigma_2^* \dot{X}_s \\ &= \frac{\pi f_c \dot{X}_s}{2a\Omega_f \sin(\theta_1) + \dot{X}_s(\pi - 2\theta_1)} + \sigma_2^* \dot{X}_s, \quad \text{when } |\dot{X}_s| \leqslant a\Omega_f \\ &= f_s \operatorname{sgn}(\dot{X}_s) + \sigma_2^* \dot{X}_s, \quad \text{when } |\dot{X}_s| > a\Omega_f. \end{aligned} \tag{5.20}$$

Typical characteristics of the effective friction are plotted in Fig. 7. The parameter values are the same as used in Section 5.1. From Fig. 7, it is observed that near very low velocity region ($\ll a\Omega_f$) effective friction behaves approximately like linear viscous damping, and this low-velocity linear slope decreases with the increasing strength of fast excitation ($a\Omega_f$). One may represent this low-velocity effective friction as

$$\langle \tilde{F} \rangle = \frac{\pi f_c}{2a\Omega_f} \dot{X}_s + \sigma_2^* \dot{X}_s, \quad \text{for} \quad |\dot{X}_s| \ll a\Omega_f. \tag{5.21}$$

To verify the analytical results, numerical simulation of the system is carried out using MATLAB™ SIMULINK. For numerical simulation, the full friction model with the Stribeck effect is considered. The slow excitation is modelled as $1.7\sin(0.5\tau)$ and the fast excitation as $1500\sin(2000\tau)$. The effective friction force vs. velocity characteristics is constructed using the filtered versions of velocity and friction. Low-pass Butterworth analog filters (filter order 8 and lower band edge frequency 500) are used to eliminate the high-frequency Components of velocity and friction signals. Numerically simulated (using Dormand–Prince algorithm) effective friction characteristics are depicted in Figs. 8(a) and (b) for two different values of v_d^*. From these figures, it is observed that low-velocity effective friction resembles linear viscous characteristics as given by Eqs. (5.20) and (5.21).

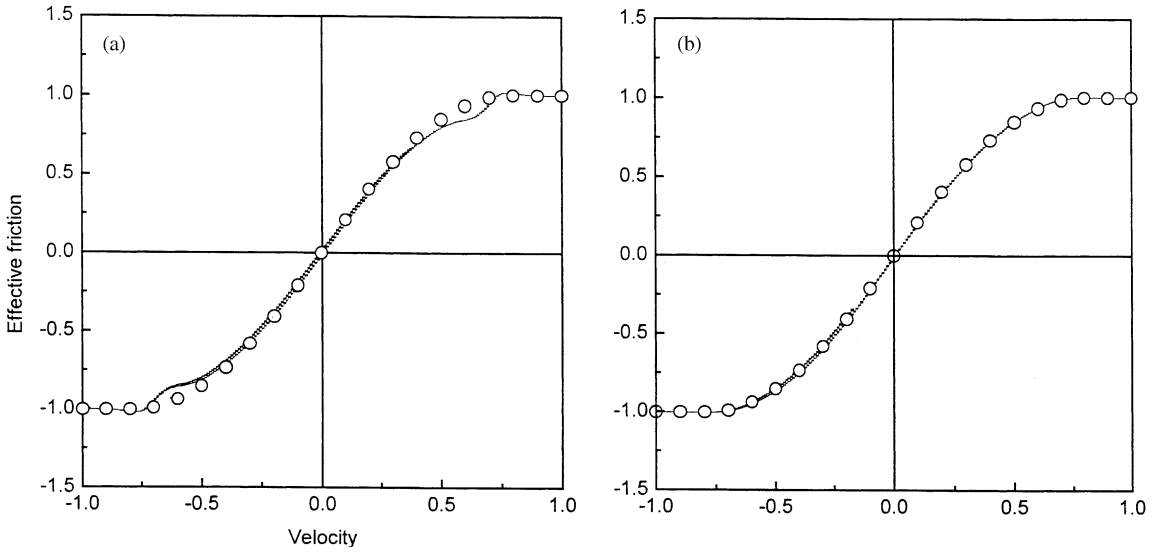

Fig. 8. Comparison of analytical and simulated effective friction for sinusoidal dither. ——, MATLAB™ simulation; ○, analytical. (a) $v_d^* = 0.1$, (b) $v_d^* = 0.01$.

6. Effect of fast vibration on stick–slip instability

In this section, the effect of fast excitation on the stability of the system (the stability of the reference state of the system) depicted in Fig. 3 is discussed. For this purpose, command velocity is considered as constant, and equation of motion of the system is rewritten in the following non-dimensional form:

$$\dot{Z} = v - \frac{\sigma_0^*|v|}{g^*(v)}Z, \tag{6.1}$$

$$\dot{e} = v_{ref} - v, \tag{6.2}$$

$$\dot{v} = e - \tilde{F} + \tilde{f}_f(\tau, T_0), \tag{6.3}$$

where

$$v = \dot{X} \quad \text{and} \quad v_{ref} = v_m^*.$$

Under the action of a dither discussed in Section 5.1, the average slow dynamics of the system is given by following non-dimensional equation of motion:

$$\dot{Z} = v - \frac{\sigma_0^*}{2}\left\{\frac{|v+W|}{g^*(v+W)} + \frac{|v-W|}{g^*(v-W)}\right\}Z = f_1(v, Z, e), \tag{6.4}$$

$$\dot{e} = v_{ref} - v = f_2(v, Z, e), \tag{6.5}$$

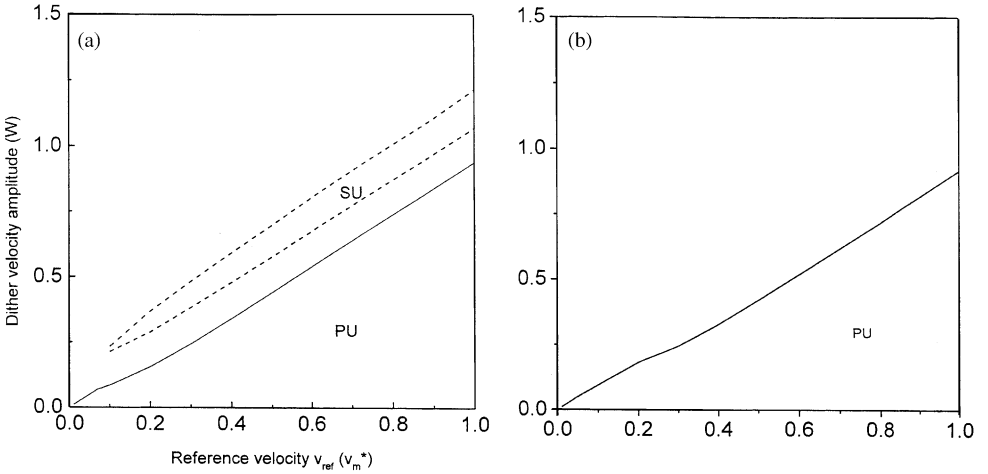

Fig. 9. Stability chart with fast excitation. Region below ——: primary unstable zone (PU), region between ------: secondary unstable zone (SU). (a) $v_d^* = 0.1$, (b) $v_d^* = 0.01$.

$$\dot{v} = e - \sigma_0^* Z - \sigma_2^* v - \frac{1}{2}\left[\sigma_1^*(v+W)\left\{(v+W) - \frac{\sigma_0^*|v+W|}{g^*(v+W)}Z\right\} + \sigma_1^*(v+W)\left\{(v-W) - \frac{\sigma_0^*|v-W|}{g^*(v-W)}Z\right\}\right] = f_3(v, Z, e). \tag{6.6}$$

The equilibrium configuration of the system is obtained as

$$Z = Z_0 = \frac{2v_{ref}}{\sigma_0^*\left\{\dfrac{|v+W|}{g^*(v+W)} + \dfrac{|v-W|}{g^*(v-W)}\right\}},$$
$$e = e_0 = \sigma_0^* Z_0,$$
$$v = v_0 = v_{ref}. \tag{6.7}$$

The stability of the system can be analyzed by computing the eigenvalues of the following Jacobian matrix:

$$\begin{bmatrix} \dfrac{\partial f_1}{\partial Z} & \dfrac{\partial f_1}{\partial e} & \dfrac{\partial f_1}{\partial v} \\ \dfrac{\partial f_2}{\partial Z} & \dfrac{\partial f_2}{\partial e} & \dfrac{\partial f_2}{\partial v} \\ \dfrac{\partial f_3}{\partial Z} & \dfrac{\partial f_3}{\partial e} & \dfrac{\partial f_3}{\partial v} \end{bmatrix}$$

at $Z = Z_0$, $e = e_0$ and $v = v_{ref}$. The system is stable when the real parts of all the eigenvalues lie in the left half of the complex plane.

As examples, stability charts in v_{ref} vs. W plane are depicted in Figs. 9(a) and (b). The stability chart is plotted only in the region of reference velocity for which the un-dithered system is

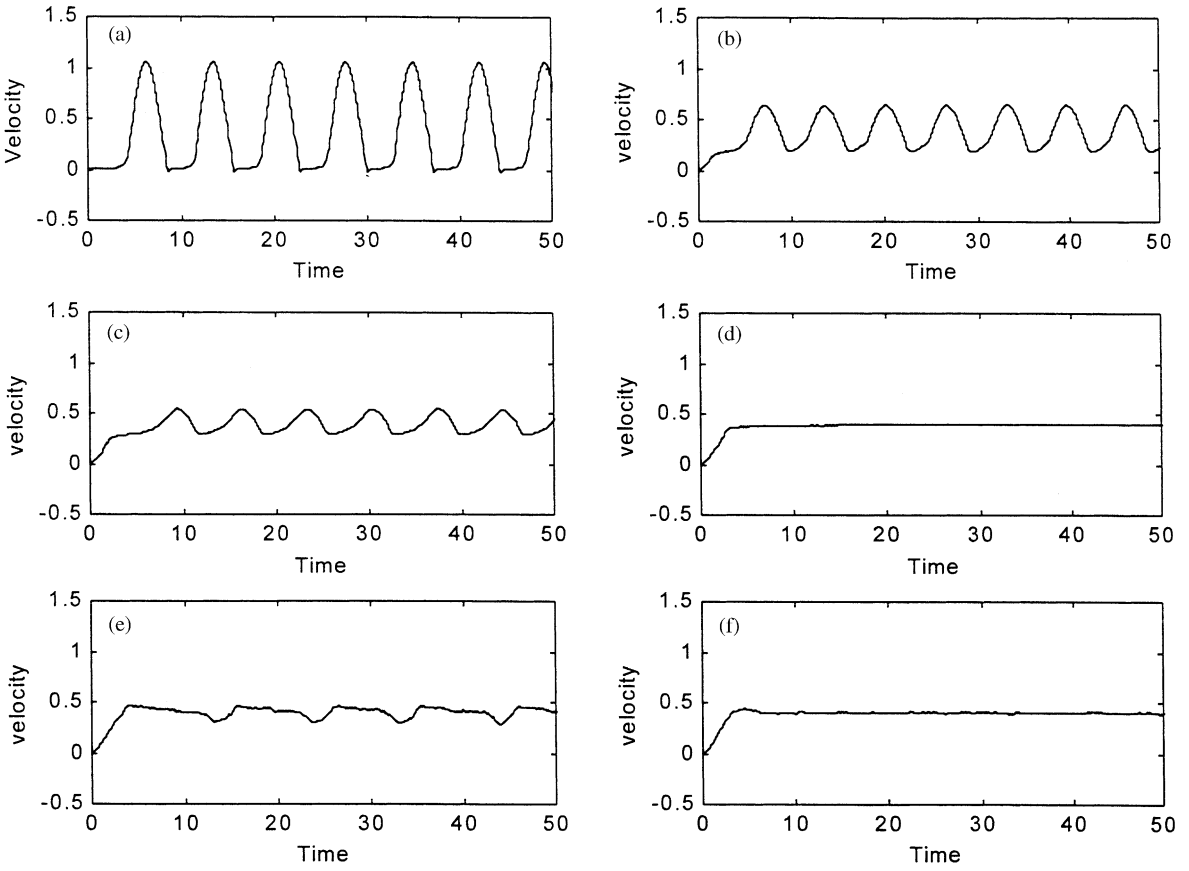

Fig. 10. Numerically simulated velocity history for different level of dither velocity amplitude. $V_{ref} = 0.4$, dither frequency = 1000. (a) $W = 0$, (b) $W = 0.2$, (c) $W = 0.3$, (d) $W = 0.4$, (e) $W = 0.5$, (f) $W = 0.6$.

unstable. From Fig. 9(a), one observes two regions of instability. The major area of instability extends over the whole range of reference velocity, and the minor zone of instability exists in the higher range of reference velocity. The minor zone of instability is associated with the secondary negative slope in the effective friction characteristics shown in Fig. 5(a). However, as shown in Fig. 9(b), the minor instability zone disappears for smaller values of v_d^*. In general, it is concluded that properly selected fast excitation stabilises friction-induced instability. It may be further noted that in the velocity region as low as the characteristic velocity v_s, fast vibration having velocity amplitude (W) greater than the reference velocity can stabilise the system.

Numerical simulation of the model is carried out for different levels of the dither velocity W and the corresponding velocity time histories of the slider are plotted in Figs. 10(a)–(f). From Figs. 10(a)–(f), it is observed that the self-sustained velocity oscillation can be either quenched or reduced by high-frequency dither. Upon proper choice of the dither frequency complete quenching of oscillation is possible (Figs. 10(d) and (f)).

7. Effect of fast vibration on stick–slip motion: numerical simulation

Analytical and numerical results discussed in the previous sections have demonstrated that fast vibration stabilises friction-induced instability by converting the negatively sloped low-velocity friction characteristics to positively sloped viscous damping. The effective friction characteristics under the action of fast vibration are also computed analytically. Though the smoothening of friction characteristics at low velocity and the corresponding effect on the stability of the system is mathematically understood, no light has so far been shed on the exact mechanism of the process. In this section, numerical study is carried out to understand the mechanism of the action of the fast vibration. For this purpose, a slightly generalised representation of the LuGre friction model, known as the elasto-plastic model [3], is taken into consideration. As described in Eq. (2.3), the elasto-plastic model of friction is different from the LuGre model only with respect to the function $\alpha(z, v)$, henceforth termed as elasto-plastic function (EP-function). Introduction of the EP-function makes it possible to detect the phases of motion like sticking ($\alpha = 0$), pre-sliding ($0 < \alpha < 1$) and sliding ($\alpha = 1$) rigorously. It is also understood that fast vibration acts through high-frequency variation of the relative velocity at the friction interface. Thus, without any loss of generality one may replace the high-frequency forcing term in Eq. (4.1) by a high-frequency velocity variation superimposed on the slow velocity of the slider. Such an action causes two-fold computational convenience. Firstly, the computation time is reduced. Secondly, full control on the dither velocity, the primary variable deciding the extent of the

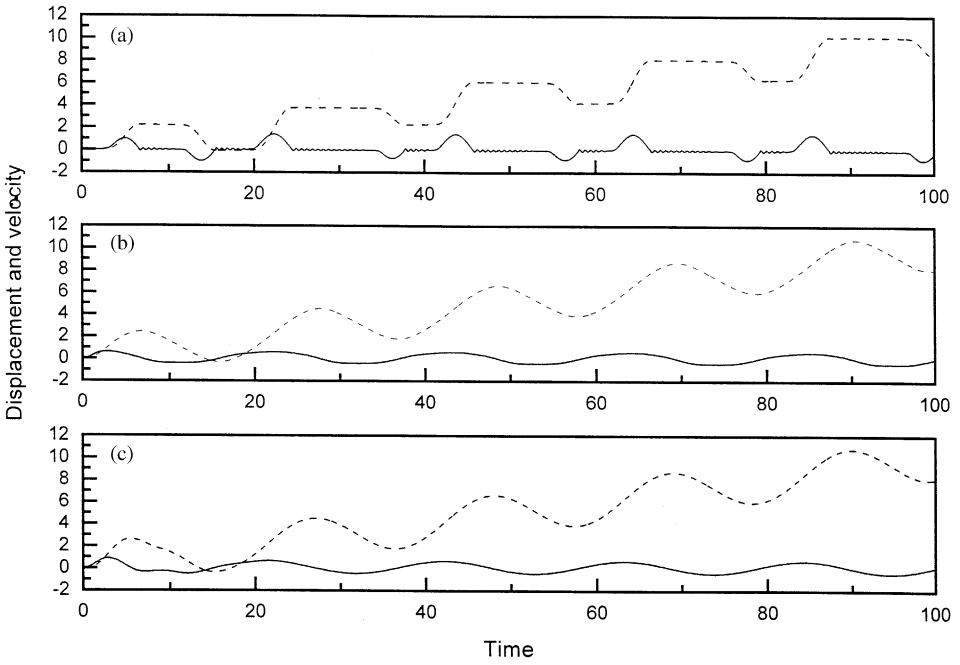

Fig. 11. Displacement and velocity time histories of the slider mass with and without fast excitation. ----, displacement; ——, velocity. (a) without dither, (b) dither amplitude = 1.5, dither frequency = 100, (c) dither amplitude = 2.5, dither frequency = 100.

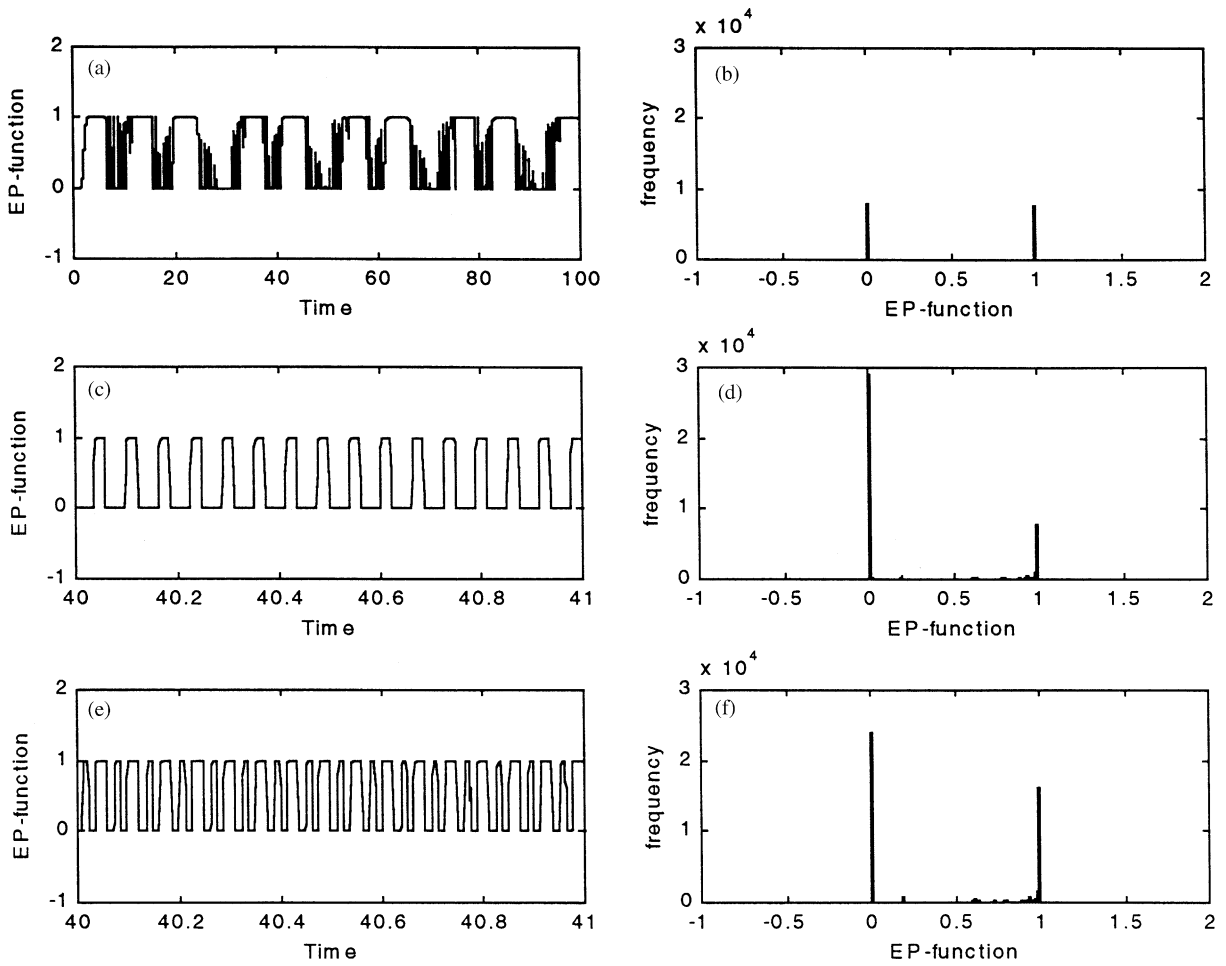

Fig. 12. Time evolution of the EP-function and the corresponding sample histograms with and without fast excitation (a) and (b) without dither, (c) and (d) dither amplitude = 1.5, dither frequency = 100, (e) and (f) dither amplitude = 2.5, dither frequency = 100.

effect, is possible. In light of the above discussion, a MATLAB™ SIMULINK model is developed for numerical simulation.

Numerical simulation is carried out using the Dormand–Prince algorithm (ODE45), a subroutine built in MATLAB, for the same parameter values as described in Sections 5.1 and 5.2. Other parameter values are as follows:

$$v_m^* = 0.1, \tilde{f}_s(\tau) = 1.7\sin(0.3\tau), \lambda = \frac{z_{ba}}{z_{ss}} = 0.8.$$

Numerically simulated time histories of displacement and filtered (low pass) velocity are presented in Figs. 11(a)–(c). Time evolution of the EP-function $\alpha(.)$ and the corresponding histogram of the sample values of $\alpha(.)$ are plotted in Fig. 12(a)–(f). The time history of the EP-function without the action of dither shown in Fig. 12(a) demonstrates the existence of long-duration sticking and

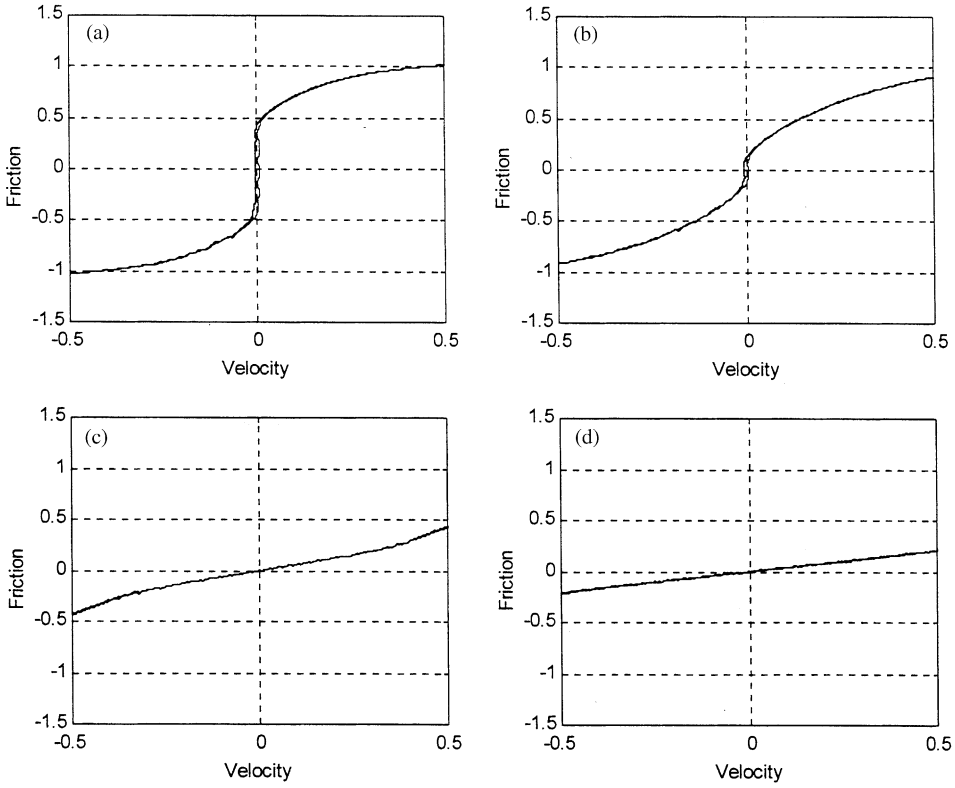

Fig. 13. Numerically simulated effective friction plot. $v_m^* = 0$. (a) dither velocity = 0.5, (b) dither velocity = 0.8, (c) dither velocity = 1.5, (d) dither velocity = 2.

slipping phases interposed by pre-sliding phases. From the corresponding histogram shown in Fig. 12(b), one concludes that the sticking and slipping phases have almost equal share out of the total number of 18 805 samples. From Figs. 12(c) and (e), one observes that under the action of dither, long-duration stick–slip is replaced by short-duration stick–slip phases. Corresponding histograms are plotted for samples taken over integration time (100). 50 162 and 55 937 number of samples are used in Figs. 12(d) and (f), respectively. From Figs. 12(d) and (f), one may conclude that the relative share of the slipping time increases with the strength of the dither.

The effective friction curves are plotted in Figs. 13(a) and (d), for different velocity amplitudes of dither with a fixed frequency of 100. One observes zero-velocity vertical line in the effective friction plots shown in Figs. 13(a) and (b), and this indicates the existence of long-duration sticking phases in the motion history. The extent of the vertical line along the friction axis represents the extent of friction force during stiction. Obviously, the extent of sticking force decreases with the increasing strength of dither. When the strength of fast excitation is strong enough, sticking phases disappear, and the corresponding low-velocity effective friction curves resemble linear viscous damping characteristics as observed in Figs. 13(c) and (d). When the dither amplitude is kept fixed and the frequency is changed, it is observed that the stick–slip motion reappears after a critical value of dither frequency, which is a function of dither velocity amplitude. Fig. 14 depicts the region of long-duration stick–slip motion in the dither amplitude vs.

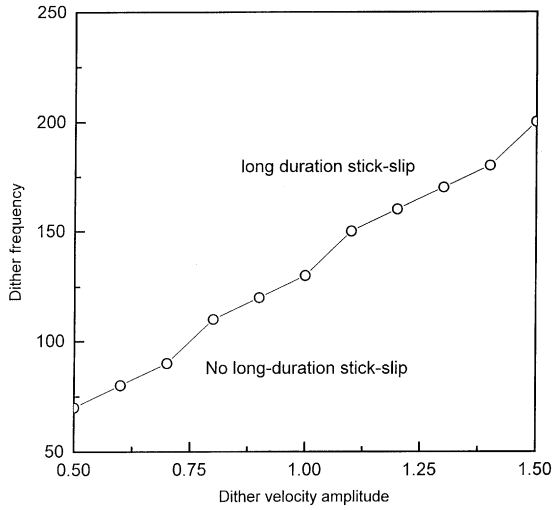

Fig. 14. Stick–slip zone in dithered system for the elasto-plastic model.

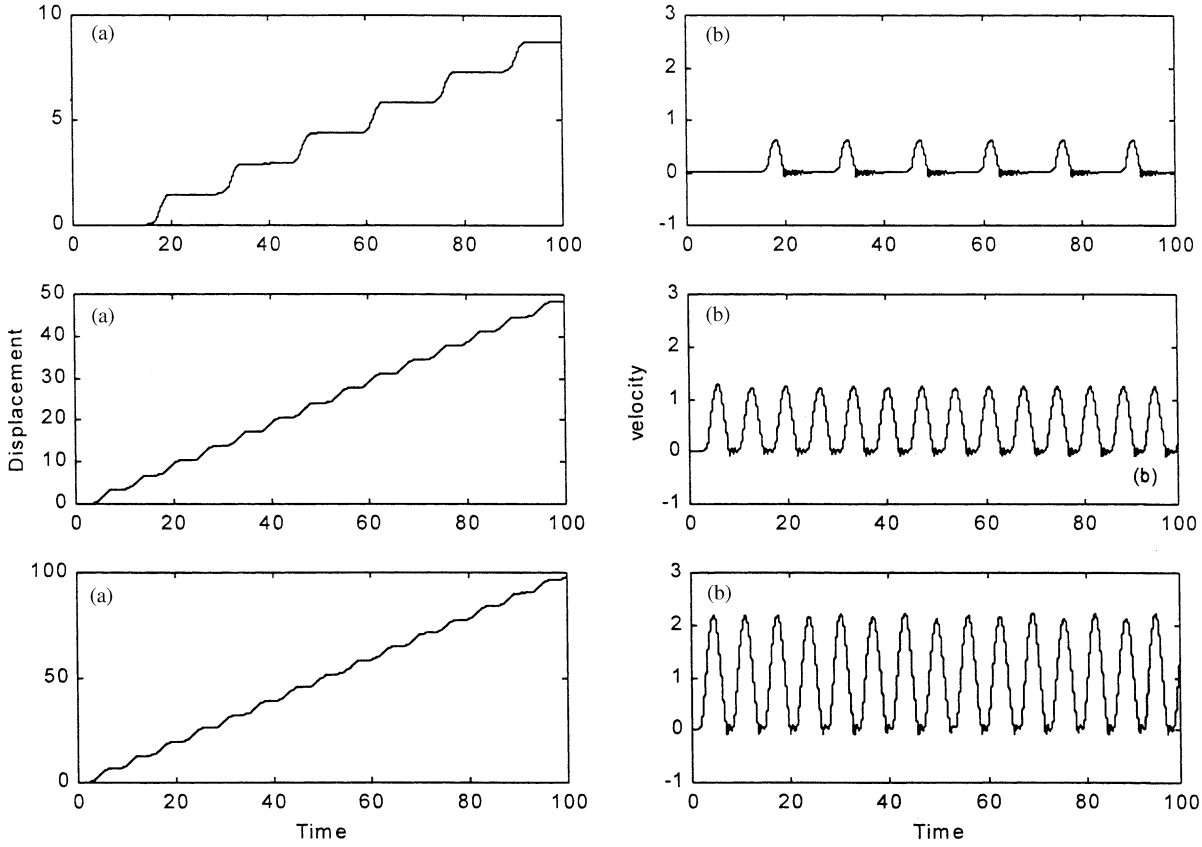

Fig. 15. Displacement and velocity histories of the system without fast excitation. (a) and (b) $v_m^* = 0.1$, (c) and (d) $v_m^* = 0.5$, (e) and (f) $v_m^* = 1$.

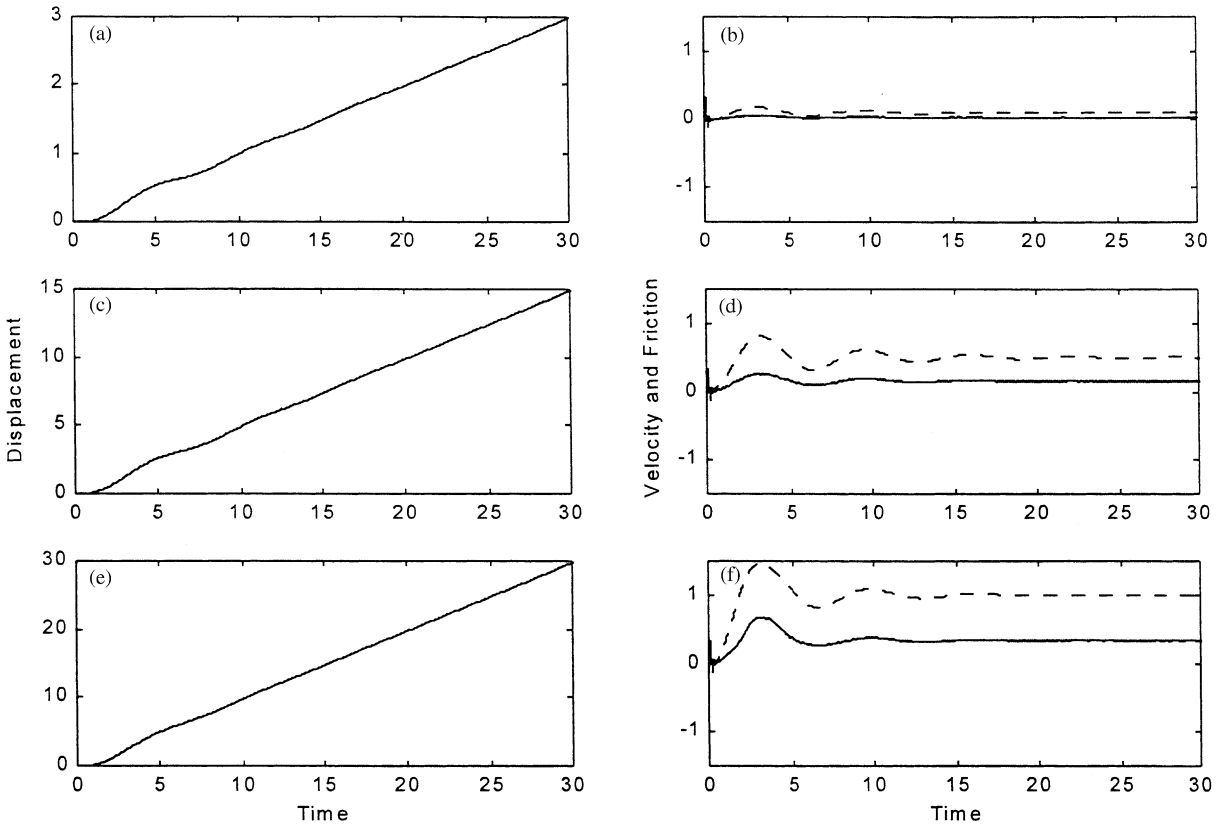

Fig. 16. Displacement and velocity histories of the system with fast excitation. ——, displacement and friction; - - - - -, velocity. (a) and (b) $v_m^* = 0.1$, (c) and (d) $v_m^* = 0.5$, (e) and (f) $v_m^* = 1$.

frequency plane. This result is in contrast to what has been observed in case of the LuGre model. However, one should keep in mind that the LuGre model does not rigorously capture the sticking phenomena.

It is interesting to understand the basic physical mechanism of the action of dither in reducing the low-velocity friction. For this purpose, the model is simulated for three different velocity commands v_m^* and without any slow excitation. Corresponding displacement, velocity and friction time histories are plotted in Figs. 15 and 16 without and with dither, respectively. From Fig. 16, one observes that long-duration stick–slip is suppressed by dither. However, as observed in Fig. 17, long-duration stick–slip phases are replaced by short-duration stick–slip phases. As friction force during sticking depends on the duration of stiction, a reduction in friction force is observed in dithered system. However, histograms of the collected samples of the EP-functions clearly show that the total relative duration of the short-time sticking phase increases with the command velocity, which is also the steady state sliding velocity of the system with dither. This accounts for the increase of friction force with the sliding velocity as observed in Figs. 16(b), (d) and (f).

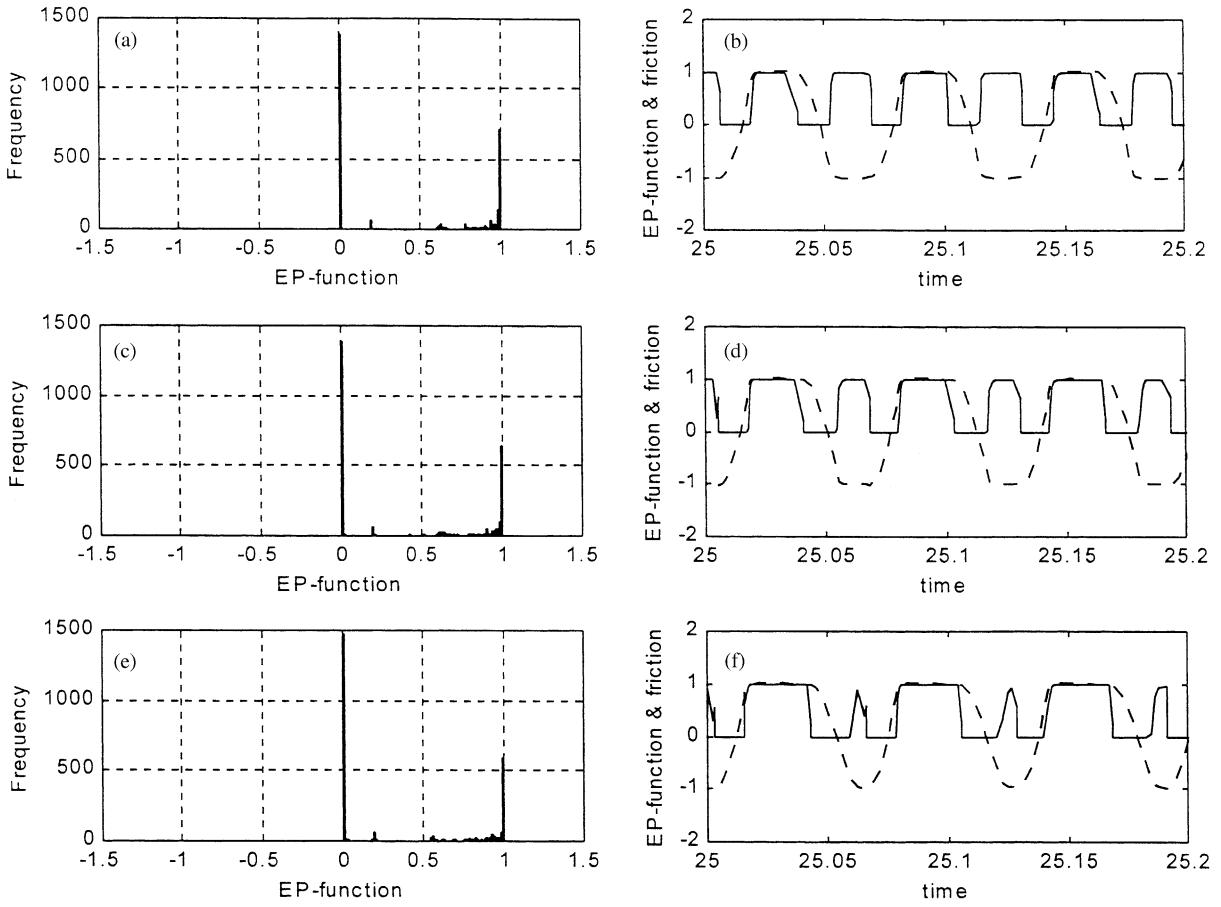

Fig. 17. High-frequency EP-function and friction time histories, and histogram of the system with fast excitation. ——, EP-function; - - - - -, friction. (a) and (b) $v_m^* = 0.1$, (c) and (d) $v_m^* = 0.5$ (e) and (f) $v_m^* = 1$.

8. Conclusions

The present paper deals with the effect of fast vibration, so-called dither, on a class of systems with friction. The interaction of microscopic and macroscopic degrees of freedom are considered for analytical and numerical investigations. The LuGre and the more rigorous elasto-plastic models are considered as the models of friction. Analytical expressions are obtained for the effective friction characteristics for two types of dither namely, square-pulse type velocity excitation and sinusoidal force excitation. Numerical simulation in MATLAB verifies the analytical results. The effective friction characteristics are shown to resemble to linear viscous damping characteristics at very low velocity. The low-velocity effective-friction characteristics depend mostly on the Coulomb friction force and the dither characteristics. The low-velocity effective-friction force decreases with the increasing strength of the fast excitation. In addition to that, by proper choices of the dither characteristics, one may completely or partially remove the

negative slope in the friction-velocity characteristics. It is worth mentioning here that the phenomenon of the non-trivial change of low-velocity friction characteristics to viscous damping characteristics due to fast excitation is not a new finding of this paper. This result is also known for some macroscopic models of friction. However, in this paper it is shown that the above result also holds well when microscopic models of friction are considered. It is also shown that the steady state kinetic friction model underestimates the low-velocity effective friction characteristics as compared to the dynamic friction models. For some parameter values associated with the bristle-damping model, one may observe a secondary negative slope in the effective friction vs. velocity characteristics besides the primary Stribeck effect. The stability of a velocity tracking system with friction is discussed in light of the dither-induced effective friction characteristics. In the stability chart, two zones of instability are detected. The primary instability zone is associated with the Stribeck effect, whereas the secondary instability zone depends on the model parameters of the bristle damping. However, a proper choice of the fast excitation can always be made for which the system is stable. Finally, a MATLAB™ SIMULINK model is developed to numerically explore the basic mechanism of dither on the effective friction force as well as stick–slip dynamics of the system. It is shown that long-duration stick and slip phases are broken down to short-duration sticking and slipping phases. This accounts for the reduction of dithered friction force, because sticking force reduces with decreasing sticking time. Total relative duration of the short-time sticking phase increases with the command velocity, and this accounts for the increase of friction with sliding velocity.

Appendix A

Let bristle deflection Z be represented by a Fourier series as follows:

$$z = z_0 + \sum_{n=1}^{H} z_n \cos(n\omega t + \phi_n), \tag{A.1}$$

where H represents the number of harmonic terms.

For the LuGre model, Eq. (2.3) may re-written as

$$g(v)\frac{\mathrm{d}z}{\mathrm{d}t} = vg(v) - \sigma_0|v|z. \tag{A.2}$$

Using Eq. (A.1) one may write

$$g(v)\frac{\mathrm{d}z}{\mathrm{d}t} = A_0 + \sum_{n=1}^{H} A_n \cos(n\omega t) + B_n \sin(n\omega t), \tag{A.3}$$

where

$$A_0 = -\alpha_1 \omega \mathrm{e}^{p_1} C_0,$$

$$A_n = -(\alpha_0 \omega n Y_n + \alpha_1 \omega \mathrm{e}^{p_1} C_n),$$

$$B_n = -(\alpha_0 \omega n X_n + \alpha_1 \omega \mathrm{e}^{p_1} D_n), \quad \text{for } n = 1, 2, 3, \ldots, H$$

$$\alpha_0 = F_c,$$

$$\alpha_1 = F_s - F_c,$$

where

$$p_1 = -\frac{v_m}{v_0},$$

$$X_0 = z_0$$

$$X_n = z_n \cos(\phi_n),$$

$$Y_n = z_n \sin(\phi_n) \quad \text{for } n = 1, 2, 3, \ldots, H$$

and

$$C_0 = \sum_{n=1}^{H} n Y_n \mathrm{I}_n(p),$$

$$C_n = \sum_{j=1}^{H} j Y_j (\mathrm{I}_{n+j}(p) + \mathrm{I}_{n-j}(p)),$$

$$D_n = \sum_{j=1}^{H} j X_j (-\mathrm{I}_{n+j}(p) + \mathrm{I}_{n-j}(p)) \quad \text{for } n = 1, 2, 3, \ldots, H$$

$I_n(P)$ is the modified Bessel's function having the following integral representation:

$$\mathrm{I}_n(p) = \frac{\omega}{\pi} \int_0^{\pi/\omega} \mathrm{e}^{p \cos(\omega t)} \cos(n\omega t)\, \mathrm{d}t.$$

Similarly,

$$vg(v) = Q_0 + Q_1 \cos(\omega t) + \sum_{n=2}^{H} Q_n \cos(n\omega t), \tag{A.4}$$

where

$$Q_0 = v_m \alpha_0 + \alpha_1 v_m \mathrm{e}^{p_1} \mathrm{I}_0(p) + \alpha_1 v_a \mathrm{e}^{p_1} \mathrm{I}_1(p),$$

$$Q_1 = v_a \alpha_0 + 2\alpha_1 v_m \mathrm{e}^{p_1} \mathrm{I}_1(p) + \alpha_1 v_a \mathrm{e}^{p_1} (\mathrm{I}_2(p) + \mathrm{I}_0(p)),$$

$$Q_n = \alpha_1 v_m \mathrm{e}^{p_1} K_n + \alpha_1 v_a \mathrm{e}^{p_1} L_n, \quad n \geqslant 2,$$

where

$$k_n = 2\mathrm{I}_n(p),$$

$$L_n = \mathrm{I}_{n+1}(p) + \mathrm{I}_{n-1}(p).$$

Similarly,

$$\sigma_0|v|z = R_0 + \sum_{n=1}^{H} R_n \cos(n\omega t) + \sum_{n=1}^{H} S_n \sin(n\omega t), \tag{A.5}$$

where

$$R_0 = \sigma_0 v_m X_0 + \sigma_0 \left(\frac{v_a}{2}\right) Y_1,$$

$$R_n = \sigma_0 v_m X_n + \sigma_0 v_a X_{n-1}\delta_{n1} + \sigma_0 \left(\frac{v_a}{2}\right) X_{n-1} U(n-1) + \sigma_0 \left(\frac{v_a}{2}\right) X_{n+1} U(H-n),$$

$$S_n = \sigma_0 v_m X_n - \sigma_0 \left(\frac{v_a}{2}\right) Y_{n-1} U(n-1) - \sigma_0 \left(\frac{v_a}{2}\right) Y_{n+1} U(H-n),$$

where

$$\begin{aligned} U(j) &= 1 \quad \text{for } j > 0, \\ &= 0 \quad \text{otherwise}, \end{aligned}$$

and

$$\begin{aligned} \delta_{ij} &= 1 \quad \text{for } i = j, \\ &= 0 \quad \text{for } i \neq j. \end{aligned}$$

Putting Eqs. (A.3)–(A.5) in Eq. (A.2), and equating equal harmonic terms one obtains

$$A_0 = Q_0 - R_0,$$

$$A_n = Q_n - R_n,$$

$$B_n = -S_n \quad \text{for } n = 1, 2, 3, \ldots, H. \tag{A.6}$$

A compact form of Eq. (A.6) is given as

$$[A]\{\vec{\xi}\} = \{\vec{b}\}, \tag{A.7}$$

where

$$\{\vec{\xi}\} = \{X_0 X_1 \ldots X_H Y_1 Y_2 \ldots Y_H\}^{\mathrm{T}},$$

$$\{\vec{b}\} = \{Q_0 Q_1 \ldots Q_H 00 \ldots 0\}^{\mathrm{T}}.$$

Therefore, one solves Eq. (A.7) to obtain bristle deflection and friction force in Fourier series as follows:

$$z = X_0 + \sum_{n=1}^{H} X_n \cos(n\omega t) - \sum_{n=1}^{H} Y_n \sin(n\omega t) \tag{A.8}$$

and

$$F = \sigma_0 z + \sigma_1(v)\frac{\mathrm{d}z}{\mathrm{d}t} + \sigma_2 v. \tag{A.9}$$

References

[1] B. Feeny, A. Guran, N. Hinrichs, K. Popp, A historical review on dry friction and stick slip phenomena, American Society of Mechanical Engineers, Applied Mechanics Review 51 (5) (1998) 321–341.
[2] C.C. Canudas de Wit, H. Olsson, K.J. Astrom, P. Lischinsky, A new model for control of systems with friction, IEEE Transaction on Automatic Control 40 (3) (1995) 419–425.
[3] P. Dupont, V. Hayward, B. Armstrong, F. Alpeter, Single state elasto-plastic friction models, IEEE Transactions on Automatic Control 47 (5) (2002) 787–792.
[4] D.A. Haessig, B. Friedland, On the modeling and simulation of friction, American Society of Mechanical Engineers, Journal of Dynamic Systems, Measurement, and Control 32 (3) (1991) 167–196.
[5] J.J. Thomsen, Using fast vibrations to quench friction-induced oscillations, Journal of Sound and Vibration 228 (5) (1999) 1079–1102.
[6] B.F. Feeny, F.C. Moon, Quenching stick–slip chaos with dither, Journal of Sound and Vibration 237 (1) (2000) 173–180.
[7] S.L. Ipri, H. Asada, Tuned dither for friction suppression during force-guided robotic assembly, International Conference on Intelligent Robots and Systems, 5–9 August, Pittsburgh, PA, USA, 1995.
[8] W. Oppelt, A historical review of autopilot development, research, and theory in Germany, American Society of Mechanical Engineers, Journal of Dynamic Systems, Measurements, and Control (1976) 215–233.
[9] S.K. Basu, D.K. Paul, Design of Machine Tools, 2nd Ed. IBH Publishing Co., Oxford, 1983.
[10] I. Blekhman, Forming properties of nonlinear mechanical systems by means of vibration, Proceedings of IUTAM/IFToMM Symposium in Synthesis of Nonlinear Dynamical Systems, 24–25 August, Riga, Latvia, 1998, pp. 1–11.
[11] Fidlin, J.J. Thomsen, Predicting vibration-induced displacement for a resonant friction slider, European Journal of Mechanics of Solids 20 (2001) 155–166.
[12] J.J. Thomsen, Some general effects of strong high-frequency excitation: stiffening, biasing, and smoothening, Journal of Sound and Vibration 253 (4) (2002) 807–831.
[13] J.J. Thomsen, D.M. Tcherniak, Chelomei's pendulum explained, Proceedings of the Royal Society of London 457 (2001) 1889–1913.
[14] J.S. Jensen, D.M. Tcherniak, J.J. Thomsen, Stiffening effects of high frequency excitation: experiments for an axially loaded beam, American Society of Mechanical Engineers, Journal of Applied Mechanics 67 (2) (2000) 397–402.
[15] S. Chatterjee, T.K. Singha, S.K. Karmakar, Non-trivial effect of fast vibration on the dynamics of a class of non-linearly damped mechanical systems, Journal of Sound and Vibration 260 (4) (2003) 711–730.
[16] M.H. Hansen, Effect of high-frequency excitation on natural frequencies of spinning discs, Journal of Sound and Vibration 234 (4) (2000) 577–589.
[17] Elmer Franz-Josef, Nonlinear dynamics of dry friction, Journal of Physics: A 30 (1997) 6057–6063.
[18] I.I. Blekhman, Vibrational Mechanics–Nonlinear Dynamics Effects, General Approach, Applications, World Scientific, Singapore, 2000.
[19] A. Isidori, Nonlinear Control Systems, An Introduction, Springer, Berlin, 1989.